20th Australasian Fluid Mechanics Conference
Perth, Australia
5-8 December 2016

Flow Structures of Flexible-Hinged Pitching Airfoils

E. Akoz[1], **S. Zeyghami**[1] **and K. W. Moored**[1]

[1]Mechanical Enginnering & Mechanics
Lehigh University, Bethlehem, PA 18015, USA

Abstract

Proper selection of kinematics and bending pattern of the propulsive surfaces are the key elements for utilizing fast and efficient propulsion. St number is one of the most important kinematic input parameters to a flapping system and it has been both experimentally studied and observed in nature that $0.2 < St < 0.4$ is the most efficient propulsion range. However, recent work has shown that for optimum efficiency, the St number of the system should be as high as possible without leading any seperation from the propulsive surface. The drawback of high St number flapping is that it leads to the deflection of the vortex street for rigid propulsors which reduces the propulsive performance. Nonetheless, it is reported that adding chordwise flexibility flattens the deflected jets up to $\mathrm{St} \to \infty$ limit. To study the flow structures behind flexible airfoils at high St numbers, a two dimensional boundary element fluid solver is developed and strongly coupled with a torsional spring structural model. The effect of the stiffness of the torsional spring and its location on flow structures are investigated.

Introduction

Fishes control their flexible appendages either actively or passively to propel themselves. The flexibility of the appendages has a major impact on the performance characteristics. A vast number of studies are conducted to understand the effect of especially chordwise flexibility of the propulsors and the optimum kinematics to drive them[see 14 for a review]. Gains of both thrust generation and efficiency is observed with proper selection of kinematics and structural stiffnesses which eventually dictates the bending pattern over the propulsor[2,12].

An important kinematic parameter of a flapping system is Strouhal number, which is defined as $St = fA/U$, where f is the flapping frequency of the propulsor, A is the amplitude of motion and U is the cruising speed. Experiments and data collected from nature suggested that St number of a system should be within an interval of $0.2 < St < 0.4$ for efficient propulsion[1,15]. However, Eloy in 2012 documented the St numbers of marine animals and reported that some animals swim with St numbers of well above 0.4 in their natural gaits[3]. Recently, Quinn et al. conducted an experimental optimization study on heaving and pitching panels and their observations extended the previously stated St number conservation law[11]. They documented that the efficency is globally maximized when the St number of the system is as high as possible without any seperation.

One drawback of high St number swimming is that velocity jet becomes deflected at some angle to the free-stream direction for $St > 0.4$[4]. This phenomenon reduces the performance of rigid foils. However, using flexible flap extensions at the trailing edge of the foils prevented deflected jets in the St number limit of infinity[9,13].

The flexibility of the propulsors is mostly evaluated in terms of the material properties such as elastic modulus or bending stiffness. Nonetheless, nature exhibits a vast number of different flexibility properties. It becomes complicated for engineers to generalize the flexibility properties of biology and reverse engineer it. In this respect, instead of generalizing the common sense properties, Lucas et al. looked at the bending patterns of various swimming and flying animals[7]. Based on their measurements, they reported a universally observed propulsor bending pattern. The flexion ratio of the propulsor is confined to a narrow interval of 0.55 <flexion ratio< 0.75, where flexion ratio is defined as the ratio of the length from propulsor's leading edge to the inflexion point to the total length of the propulsor in spanwise direction. Recently, Lucas et al. extended this finding to the chordwise direction by conducting experiments on functionally graded, heaving and pitching panels[8]. The optimum efficiency is observed for 2/3 rigid, 1/3 flexible panel which gives a chordwise flexural stiffness of 2/3.

In light of the above observations, we conducted a computational study to compare the flow structures of rigidly heaving airfoils and flexible-hinged pitching airfoils. Different hinge points, as flexion ratios, and various flexibilities are investigated to understand the neutralization of the deflected jet characteristics.

Analysis

Computational Model and Validation

To model a high Reynolds number fluid flow around the airfoils, the flow field is modeled as a potential flow. In the potential flow approximation, the continuity equation reduces to the Laplace's equation, $\nabla^2\phi = 0$. Following Katz&Plotkin, the solution to Laplaces equation is found by distributing source and doublet singularities on the problem boundaries[5]. The boundary conditions of the problem are;(1) the velocity component normal to the body's surface must be zero(no-flux boundary condition), (2) the disturbance created by the flow should decay far from the body(far-field boundary condition). The elementary solutions of the doublet and source both automatically fulfill the far-field boundary condition. No-flux boundary condition requires constant velocity potential inside the boundaries. Therefore, a general solution to the Laplace's equation can be written for an arbitrary point(P) within the flowfield as;

$$\phi_i(P) = \frac{1}{2\pi}\oiint_{S_B}[\sigma(lnr) - \mu\frac{\partial(lnr)}{\partial n}]dS - \frac{1}{2\pi}\oiint_{S_W}\mu\frac{\partial(lnr)}{\partial n}dS$$

where σ and μ are the strengths of source and doublet elements on the boundaries, respectively and $\phi_i(P)$ is the velocity potential of an arbitrary point within the boundaries. Setting the internal velocity potential to zero, $\phi_i(P) = 0$, reduces the solution to finding the strengths of the sources and doublets over the known boundaries. To solve the problem numerically, the geometry is divided into N panels, as shown in the Figure 1, and the integration is performed for each panel such that;

$$\sum_{j=1}^{N} B_j\sigma_j + \sum_{j=1}^{N} C_j\mu_j = 0$$

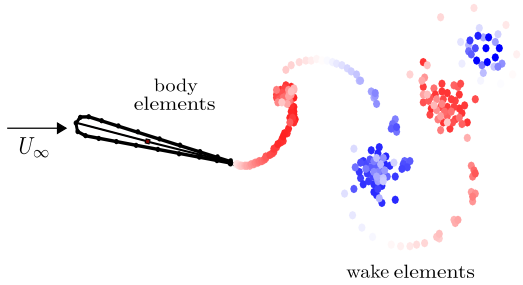

Figure 1: Illustration of a tear drop airfoil utilizing a pure pitching motion with the panel edge points are shown as dots on the surface. Different sign vortices are shown with different colors. The inflexion point where the spring is located is shown as a square on the mid-chord line.

where

$$C_j = -\frac{1}{2\pi}\int_{panel}\frac{\partial(lnr)}{\partial n}dS|_j$$

and

$$B_j = \frac{1}{2\pi}\int_{panel}(lnr)dS|_j$$

At every time step, a panel element with a known doublet strength advects from the trailing edge with local velocity, rolls up and forms vortices in the wake region(See Figure 1). During the rollup process, the ends of the wake doublet elements, which are point vortices, must be de-singularized for the numerical stability of the solution[6]. At a cutoff radius of $\varepsilon/c = 2.5\times10^{-4}$, the irrotational induced velocities from the point vortices are replaced with a rotational Rankine core model. The tangential perturbation velocity is found by local differentiation of the velocity potential. Then the pressure field acting on the body is calculated using unsteady Bernoulli equation.

A torque balance is forced on the leading edge of the airfoil to calculate the final position of the airfoil at each time step. Structural solver iterates the the airfoil position until the torque balance of inertial, fluid and spring forces is satisfied. An Aitken adaptive under relaxation method is used to prevent numerical instabilities and guarantee convergence.

The in-house developed solver is validated against an analytic model, so called torsional flexibility model, where a torsional spring is attached to the leading edge of a rigid airfoil. Nick Moore obtained exact solutions for thrust and power by linearizing incompressible Euler equations using small amplitude motion assumption[10]. For the validation cases, we actively controled the leading edge of the thin airfoil with a small amplitude heaving motion and trailing edge followed with passive pitching. The results are shown in Figure 2 for 3 different K values, which is a non-dimensional parameter, measures the spring stiffness compared with fluid forces; $K = \kappa/\rho U_\infty^2 c^2$, where κ is the torsional spring constant, ρ is the fluid density, U_∞ is the fre-stream velocity and c is the chord length. We observed a remarkable collapse of our simulation results with the analytical model, for both thrust and power coefficients as the non-dimensional driving frequency, σ, is varied, $\sigma = \pi f c/U_\infty$.

Problem Formulation

Computations are performed on two-dimensional 5% thick teardrop airfoils undergoing pitching motion. The flow structure of functionally graded airfoils are compared against rigid airfoils. Functionally graded airfoils are modelled as a rigid leading edge side and a passively pitching trailing edge side. A hinge point or the inflexion point, which is modelled with a torsional spring, is seperating the rigid and the passively pitcing parts. Two different flexion ratios(0.3-0.7) are studied among with the rigidly pitching airfoil at a fixed St number(0.5), where St number is defined based on the rigid's airfoil tip-to-tip amplitude. The torsional spring constant(κ) is also varied to understand the effect of flexibility of the hinged portion on the flow structures.

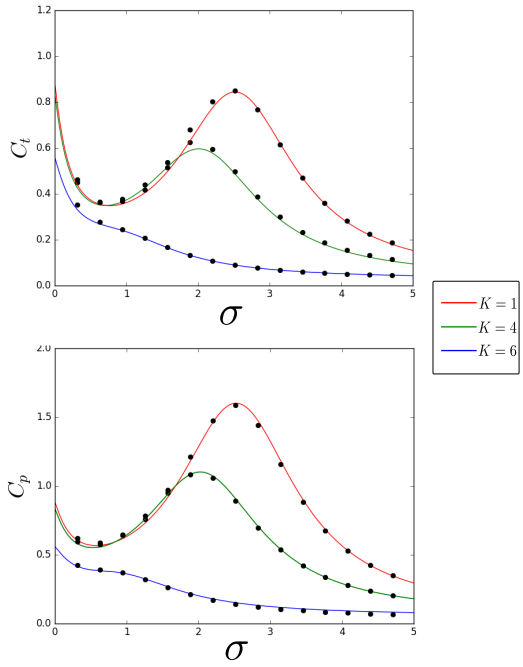

Figure 2: Coefficent of thrust and power as a function of reduced frequency. Solid lines show the analytical results for 3 different K values and black dots are our simulation results

For all computations, frequency of pitching and free-stream velocity are set to $f = 1Hz$ and $0.1m/s$, respectively. A virtual drag law is applied on airfoils to satisfy a steady state solution in an inviscid environment. For high Reynolds numbers, drag law is $D = \frac{1}{2}C_d S_w U^2$ where ρ is the density of the fluid, C_d is the coefficient of drag, S_w is the wetted surface area and U is the free-stream velocity.

Results and Discussion

Jet deflection behind the airfoils at high St numbers reduces the performance of propulsors. In literature, deflected jets started to be seen for St numbers larger than 0.4[4]. To prevent jet deflection at the operating St number of 0.5, we introduced a hinge point to a rigid airfoil and study the functioanally graded material effects on flow structures.

In Figure 3(a), for the rigid airfoil, it is clear that the vortex street is at an angle to the horizontal axis. Two different flexion ratios, 70% and 30%, and the flow field behind them are seen in Figure 3(b) and 3(c), respectively. A K value of 6 is selected for both cases. Two snapshots of the same airfoil represent two phases that are π radians apart in the same cycle. The deflection is recovered with the addition of the passively pitching part for both cases. The mechanism of recovery, however, is different. In the case 70% rigid airfoil, trailing edge amplitude is small compared to the driving amplitude all over the cycle. Thus, vortices form a straight street in between the narrow amplitude range of the trailing edge. In the 30% rigid case, on the other hand, trailing edge undergoes a larger amplitude motion. Initial width of the vortex street is larger in compared to the 70% rigid

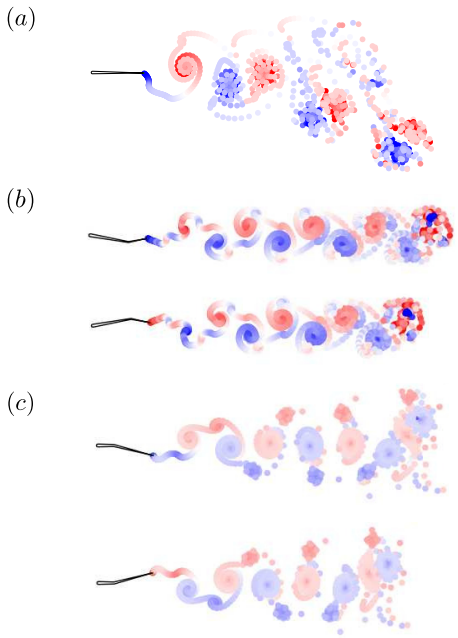

Figure 3: The comparison of a rigidly pitching airfoil(a), with airfoils of different flexion ratios; 0.7(b) and 0.3(c). Two snapshots are taken π radians apart in the same cycle. St number is fixed at 0.5 and a K value of 4 is used for the airfoils with the hinge points

case and eventually jet width grows with a higher rate as well. The flowfield resembles the Shinde and Arakeri's experimental observations[13]. The duration of the trailing edge excursion from one end to the other is greater than the rigid airfoil's travelling time. This allows more time for the shed vortices to convect further downstream which in turn prevents the dipole formation and jet inclination. Furthermore, for both hinge point locations, each time the trailing edge changes direction, one strong vortex and a weak same sign vortex are shed.

Investigating the natural frequencies of the foils with different inflexion points explains the contrast observed in trailing edge amplitudes. Nick Moore documented a fast way to calculate the resonant frequency of a flapping wing which, as well, can be used in our case[10];

$$f_r \sim \frac{1}{2\pi}\sqrt{\frac{\kappa}{I+I_a}}$$

where I is the airfoil's moment of inertia and I_a is the added fluid inertia for a thin plate rotated about an endpoint which is approximated as $I_a = 9\pi l^4/128$ in our case(l is the length from the hinge point to the trailing edge). We found out that the natural-resonance frequency of the 70% rigid airfoil is more than 9 times larger than the driving frequency. This small ratio of f/f_r leads to small amplitude pitching response of the trailing edge. However, for the 30% rigid case, $f/f_r \approx 0.5$ which yields a maximum trailing edge amplitude of the same order with the input driving amplitude.

Since the driving frequency is well below the resonance frequency in the first set of simulations, we chose a lower K value of 1 to understand the flow response at around resonance frequency of the system. The same St number and inflexion points are used for the next set of experiments. In Figure 4(a) and 4(b) two snapshots are shown associated to the 70% and 30% rigid airfoils. For the 70% rigid case, the $f/f_r \approx 0.6$ which explains

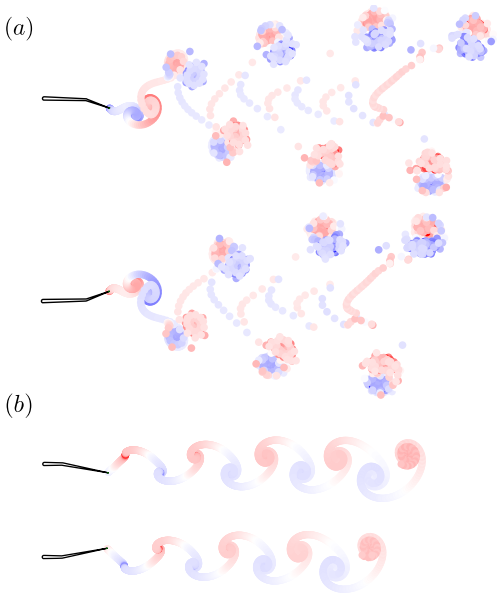

Figure 4: Comparison of airfoils with two different flexion ratios of 0.3 and 0.7. St number is fixed to 0.5 and a K value of 1 is used for both cases. Snapshots are taken π radians apart in the same cycle.

the large amplitude pitching of the trailing edge. The flowfield becomes staggered and for each time trailing edge changes direction, a pair of relatively same strength vortices is being shed which makes positive and negative angles to the horizontal axis. Flow field resembles a 90° rotated growing v letters in downstream direction, where each v is associated to another oscillation cycle.

For the 30% rigid case, f/f_r ratio goes above 1 and is approximately 1.4. Once the driving frequency passes the resonance frequency of the system, flow field becomes more stable. At every extreme of pitching, one strong vortex is being shed. Overall, flow field resembles a reverse Bernard von-Karman vortex street.

Conclusion

In conclusion, in consistent with the previous literature, we observed that adding a flap like passively pitching portion to a rigid airfoil prevents the jet deflection. The mechanisms stabilize the vortex street, however, are different. Driving the airfoil well below its resonance frequency leads to a narrow jet due to the small amplitude motion of the trailing edge. This, in turn, restricts the vortex shedding to a small width and flattens the jet. On the other hand, driving the airfoil at or around the resonance frequency of the structure leads to a wider wake. Since the trailing edge excursion is larger in compared to the rigid airfoil case, this extra time in between successive sheddings, allows the vortices to be apart of each other. This mechanism eventually prevents the dipole formation and jet inclanation.

As f/f_r is systematically decreased an interesting pattern is observed on the flow structures. Once the ratio is on the order of 0.5 or smaller, a strong and a weak same sign vortices are shed at every time trailing edge changes direction. Further increasing the ratio, flow field first resembles 90° rotated growing v letters where a pair of counter rotating vortices at the extremes of the oscillations. Finally, going above the structural resonance frequency leads the flow field to become a reverse Bernard von-Karman vortex street.

Acknowledgements

This work was supported by the Office of Naval Research under Program Director Dr R. Brizzolara, MURI grant number N00014-14-1-0533.

References

[1] Anderson J. M., K. Streitlien, D. S. Barret, and M. S. Triantafyllou, J. Fluid Mech. 360, 41 (1998).

[2] Dai, H., Luo, H., de Sousa, P. J. F., Doyle, J. F. (2012). Thrust performance of a flexible low-aspect-ratio pitching plate. Physics of Fluids (1994-present), 24(10), 101903.

[3] Eloy, Christophe. "Optimal Strouhal number for swimming animals." Journal of Fluids and Structures 30 (2012): 205-218.

[4] Godoy-Diana, Ramiro, Jean-Luc Aider, and Jos Eduardo Wesfreid. "Transitions in the wake of a flapping foil." Physical Review E 77.1 (2008): 016308.

[5] Katz, J., Plotkin, A. (2001). Low-speed aerodynamics (Vol. 13). Cambridge University Press.

[6] Krasny, R. (1986). A study of singularity formation in a vortex sheet by the point-vortex approximation. Journal of Fluid Mechanics, 167, 65-93.

[7] Lucas, Kelsey N., et al. "Bending rules for animal propulsion." Nature communications (2014).

[8] Lucas, Kelsey N., et al. "Effects of non-uniform stiffness on the swimming performance of a passively-flexing, fish-like foil model." Bioinspiration biomimetics 10.5 (2015): 056019.

[9]Marais, C., Thiria, B., Wesfreid, J. E., Godoy-Diana, R. (2012). Stabilizing effect of flexibility in the wake of a flapping foil. Journal of Fluid Mechanics, 710, 659-669.

[10] Moore, M. Nicholas J. "Analytical results on the role of flexibility in flapping propulsion." Journal of Fluid Mechanics 757 (2014): 599-612.

[11] Quinn, Daniel B., George V. Lauder, and Alexander J. Smits. "Maximizing the efficiency of a flexible propulsor using experimental optimization." J. Fluid Mech 767 (2015): 430-448.

[12] Ramananarivo, S., Godoy-Diana, R., Thiria, B. (2011). Rather than resonance, flapping wing flyers may play on aerodynamics to improve performance. Proceedings of the National Academy of Sciences, 108(15), 5964-5969.

[13] Shinde, Sachin Y., and Jaywant H. Arakeri. "Flexibility in flapping foil suppresses meandering of induced jet in absence of free stream." Journal of Fluid Mechanics 757 (2014): 231-250.

[14] Shyy, W., Aono, H., Chimakurthi, S. K., Trizila, P., Kang, C. K., Cesnik, C. E., Liu, H. (2010). Recent progress in flapping wing aerodynamics and aeroelasticity. Progress in Aerospace Sciences, 46(7), 284-327.

[15] Taylor G. K., R. L. Nudds, and A. L. R. Thomas, Nature (London) 425, 707 (2003).